Integrated Systems and Technologies: Mathematical Oncology

Cancer Research

Antigen Shedding May Improve Efficiencies for Delivery of Antibody-Based Anticancer Agents in Solid Tumors

Youngshang Pak[1], Yujian Zhang[2], Ira Pastan[2], and Byungkook Lee[2]

Abstract

Recombinant immunotoxins (RIT) are targeted anticancer agents that are composed of a targeting antibody fragment and a protein toxin fragment. SS1P is a RIT that targets mesothelin on the surface of cancer cells and is being evaluated in patients with mesothelioma. Mesothelin, like many other target antigens, is shed from the cell surface. However, whether antigen shedding positively or negatively affects the delivery of RIT remains unknown. In this study, we used experimental data with SS1P to develop a mathematical model that describes the relationship between tumor volume changes and the dose level of the administered RIT, while accounting for the potential effects of antigen shedding. *Cancer Res; 72(13); 3143–52. ©2012 AACR.*

Major Findings

We found that antigen shedding is a favorable biologic process for targeted therapy of solid tumors. Shed antigens acted as a protective reservoir of RIT and buffered against the well-known binding site barrier effect, promoting a more uniform distribution of RIT in the tumor. In addition, our model reproduced the decrease in tumor size upon RIT treatment in animal experiments. Our findings, therefore, can be used to study the delivery efficacy of RITs and also antibody–drug conjugates currently in clinical trials.

Introduction

Many anticancer agents are composed of antibodies attached to cytotoxic drugs or protein toxins (1, 2). They bind to the specific target antigen on the surface of cancer cells and then are internalized and processed to release the cytotoxic component within the target cell. Generally, they work better on leukemias than against solid tumors, because of factors in solid tumors that are known to limit the entry and dispersal of these agents. The physical process of the delivery of the antigen-targeting agents through the solid tumor tissue has been the subject of numerous studies and several reviews are available (3–7).

Authors' Affiliations: 1Department of Chemistry and Institute of Functional Materials, Pusan National University, Busan, Republic of Korea; and 2Laboratory of Molecular Biology, National Cancer Institute, NIH, Bethesda, Maryland

Note: Supplementary data for this article are available at Cancer Research Online (http://cancerres.aacrjournals.org/).

Corresponding Authors: Byungkook Lee, NIH, Bldg. 37, Room 5120, 37 Convent Drive, MSC 4264, Bethesda, MD 20892. Phone: 301-496-6580; Fax: 301-480-4654; E-mail: bk@nih.gov; and Youngshang Pak, ypak@pusan.ac.kr

doi: 10.1158/0008-5472.CAN-11-3925

It is well known that many tumor-specific surface antigens, including CA125, Her-2/neu, prostate-specific antigen (PSA), carcinoembryonic antigen (CEA), and others, are actively shed from cancer cells (8). Such shedding can be expected to significantly influence the delivery of anticancer agents that use these antigens as the delivery target (9). However, no theoretical study has been reported on the effect of antigen shedding on the delivery of these agents in solid tumors.

We previously reported on a mathematical model that relates the tumor volume changes to the dose level of the administered recombinant immunotoxins (RIT; ref. 10). RITs are targeted anticancer agents and composed of a targeting antibody fragment and a protein toxin fragment. The model takes into account various physical events that the RIT encounters during its travel from the blood vessel to the cytosol of a tumor cell. The original model (10) used mass balance equations for 2 types of tumor cells, the normal and the intoxicated, using fluid-like treatment of cells (11, 12). This model reproduced the experimental volume profiles with time of human tumors growing in mice, which had been given different doses of RIT, and showed the well-known binding site barrier effect (13, 14). It also identified nearly 20 factors that were involved in the RIT trafficking process, some of which were predicted to affect the RIT-induced tumor volume change much more than others.

For the current study, we modified this original model in several different ways (see Materials and Methods), one of which was to include the effect of target antigen shedding. We apply this modified model to the specific case of SS1P (anti-mesothelin-Fv-PE38), which is one of the most extensively studied RITs. SS1P binds to mesothelin expressed on cells of several different types of solid tumors including mesothelioma, ovarian cancer, pancreatic cancer, and lung cancer (15). Currently SS1P is being evaluated for the treatment of mesothelioma (16–18).

We have shown that mesothelin is actively shed in large quantities into the extracellular space (ECS) of the tumor and into the blood (19). In the case of the mesothelin-expressing

Quick Guide to Equations and Assumptions of the Model

Tumor volume and cell composition changes

The tumor volume is obtained from the flux of cells across the outer boundary, r_o, of representative unit (RU) using:

$$\frac{dV}{V} = \frac{4\pi r_o^2 u(r_b)dt}{v'}, \tag{A}$$

where V is the tumor volume, $u(r_o)$ is the velocity of the cell flow at r_o, and $v' = \frac{4}{3}\pi(r_o^3 - r_b^3)$ is the volume of the extravascular space (EVS) of the RU, r_b being the radius of the vasculature. Note that when tumor grows (shrinks), u is positive (negative).

The density of normal tumor cells in EVS, ρ_1, is governed by:

$$\frac{\partial \rho_1}{\partial t} = U_o(\rho_1) + \Gamma \cdot \rho_1 - f \cdot \rho_1, \tag{B}$$

where

$$U_o(x) \equiv -\frac{1}{r^2}\frac{\partial}{\partial r}\left(r^2 u \cdot x\right) + [x(r_o) - x(r)]\frac{4\pi r_o^2 u(r_o)}{v'}, \tag{B'}$$

and Γ and f are the rate constants of the cell growth and the intoxication, respectively. The first term in equation (B′) represents the change in the cell density at any given point due to the cells flowing into and out of the given point. The second term in equation (B′) represents the change in the cell density (generally, any quantity x) due to the material that flows in or out of RU.

Similar expressions govern the densities of the other 2 cell types, the intoxicated and the dead cells. The cell flow velocity $u(r,t)$ is determined from the condition that the sum of these 3 densities, $\rho^* = \rho_1 + \rho_2 + \rho_3$, is constant over r or t.

The intoxication rate and the toxin concentrations inside the cell

The intoxication rate constant $f(r,t)$ in equation (B) measures the rate of conversion of type 1 to type 2 cells. It is assumed to depend linearly on the toxin concentration in the cytosol of type 1 cells and, therefore, couples the set of equations that govern the cell densities and the set of equations that govern the toxin concentrations. The toxin concentrations in the cytosol and in all other compartments within the cell, which we refer to generically as "endosome," are given by the following coupled equations:

$$\frac{\partial T_1^{cc}}{\partial t} = U_o(T_1^{cc}) + k_t \cdot T_1^{ce} - \chi_{cc} \cdot T_1^{cc} - f \cdot T_1^{cc}, \tag{C}$$

$$\frac{\partial T_1^{ce}}{\partial t} = U_o(T_1^{ce}) + k_e \cdot cR_1^{cs} - k_t \cdot T_1^{ce} - \chi_{ce} \cdot T_1^{ce} - f \cdot T_1^{ce}, \tag{C'}$$

where T_1^{cc} and T_1^{ce} are the EVS concentrations of the toxin molecules in the cytosols and in the endosomes of type 1 cells, respectively, U_o is the function defined by (B′), cR_1^{cs} is the EVS concentration of the recombinant immunotoxin (RIT)–receptor complexes on the surfaces of type 1 cells, and k_t, k_e, χ_{cc}, and χ_{ce} are the rate constants for translocation of the toxin from the endosome into the cytosol, endocytosis, toxin inactivation in the cytosol, and toxin inactivation in the endosome, respectively. Similar equations govern the toxin concentrations in type 2 and 3 cells, except that the endosome and cytosol are combined for the type 3 cells.

Receptor turnover and shedding

The RIT enters cells when the RIT–receptor complex on the cell surface enters cells through endocytosis. The receptors are removed from the surface by endocytosis and by shedding into the extracellular space (ECS) and replenished by migration to the surface from the interior of the cell (Supplementary Fig. S2). The total number of receptors (free plus RIT-complexed) on the surface of each cell is governed by the following coupled equations:

$$\frac{d(tR_i^{CS})}{dt} = -k_e \cdot tR_i^{CS} - k_s \cdot tR_i^{CS} + k_c \cdot tR_i^{C}, \tag{D}$$

$$\frac{d(tR_i^{C})}{dt} = k_e \cdot tR_i^{CS} - k_{deg} \cdot tR_i^{C} + Q_i \text{ for i} = 1, 2, \tag{D'}$$

where tR_i^{CS} and tR_i^{C} are the total number of receptors per cell on the surface and in the interior of cell type i, k_s, k_c, and k_{deg} are the rate constants for shedding, recycling (migration from inside to the surface), and degradation of receptors, respectively, Q_1 is the protein synthesis rate in cell type 1 and $Q_2 = 0$. The number of RIT–receptor complexes is obtained from the total number of receptors and the free RIT concentration in the ECS using the RIT–receptor on and off reaction rates.

The RIT concentration in the ECS

The mass balance equation for the concentration of free (uncomplexed) RIT, T, in ECS is

$$\frac{\partial T}{\partial t} = \frac{D}{r^2}\frac{\partial}{\partial r}\left(\frac{r^2 \partial T}{\partial r}\right) + U_o(T) - \chi_{ecs} \cdot T - k_a \cdot \sum_i^3 fR_i \cdot T + k_d \cdot \sum_i^3 cR_i - k_a \cdot sfR \cdot T + k_d \cdot scR, \quad \text{(E)}$$

where D and χ_{ecs} are the diffusion and the degradation rate constants of free RIT in ECS, respectively, and *sfR* and *scR* are the ECS concentrations of the shed receptors, free and complexed, respectively. The first term in this equation represents diffusion of the RIT through the ECS of the tumor tissue. The last 4 terms represent the association/dissociation reactions with the surface-bound and the shed receptors. Similar expressions govern the concentrations of the free and complexed shed receptors in the ECS.

A431 tumors, we expect the shedding rate constant to be approximately 0.4 per hour (see Materials and Methods), which is roughly comparable with the endocytosis rate of approximately 0.22 per hour that we estimate from the data of Zhang and colleagues (20). The surface mesothelin lost through shedding and endocytosis is replenished in normal tumor cells by fresh protein synthesis.

It seemed possible that the shed free mesothelin could act as a decoy in the ECS of the solid tumor, thereby reducing the free RIT concentration available for binding to the cell surface antigen. Also, the RIT bound to mesothelin on the cell surface can be released back to the ECS instead of entering the cell by endocytosis when the mesothelin is shed from the surface. Indeed, we have shown that addition of an inhibitor to the mesothelin sheddase in cell cultures reduced shedding and increased the concentration of SS1P inside the cells (19). Because of these effects, antigen shedding was expected to reduce targeting efficiency (21). Surprisingly, the model shows that antigen shedding greatly enhances, not retards, the effectiveness of the RIT in the solid tumor. The reason is, in part, that the shed antigen acts as a protective reservoir of RIT, which helps to bypass the binding site barrier (22). This finding has important implications in designing methods for an efficient delivery of this class of anticancer agents against solid tumors.

Materials and Methods

The model setup

The model treats a tumor as a collection of identical representative units (RU, Fig. 1). Each RU is a sphere of 38-μm radius and has a spherical blood vessel at its center, 3 different types of cells—the normal tumor cells (type 1), the intoxicated tumor cells (type 2) in which the protein synthesis has stopped, and the dead tumor cells (type 3) in which all biochemical processes ceased—outside of the blood vessel, and a small amount of ECS between the cells. The present model does not include nontumor cells, although such cells are known to exist in the tumor tissue (20). Future models will include these other cell types. Each cell has 3 compartments—the surface, the cytosol, and the remainder, which we designate generically as endosome—except that we combine cytosol and endosome for the dead cells.

The mathematical model consists of 2 main sets of differential equations. One set describes the kinetic steps that the RIT molecules go through within the RU from crossing the blood vessel wall into the tumor extravascular space (EVS) until they either are degraded or reach the cytosol in an active form to intoxicate the cell. These steps include (Fig. 1; Supplementary Fig. S1) permeation through the blood vessel wall to enter the tumor ECS, diffusion in the ECS between tumor cells, binding to the surface antigen, internalization by endocytosis, passage through endosomal compartments, translocation into the cytosol, and finally intoxication of the cell. These equations give the amount of RIT molecules that are present and degraded in each compartment of the tumor tissue. The other set of differential equations describes the growth, death, and movement of tumor cells within each RU and their flow in and out of the RUs. Cells move because the tumor grows and because the RIT intoxicates cells, which then die and are cleared, creating space into which neighboring cells can move. These equations give the volume and the tumor cell composition of the whole tumor at all times.

Although the current model is conceptually the same as the previous model (10), the mathematical equations were completely rewritten to incorporate 4 new features: (i) The new model allows the antigen to be shed from the surface of the normal and intoxicated tumor cells. (ii) The new model recognizes one additional cell type, the dead cells, in addition to the 2 that the previous model used. The dead cell type was introduced in this model to recognize the fact that tumor volume does not shrink immediately after the intoxicated cells die. (iii) The new model treats the antigen–antibody binding as a kinetic process, requiring the use of the on and off rate constants, rather than as an equilibrium process as was done in the original model. (iv) The new model recognizes that the

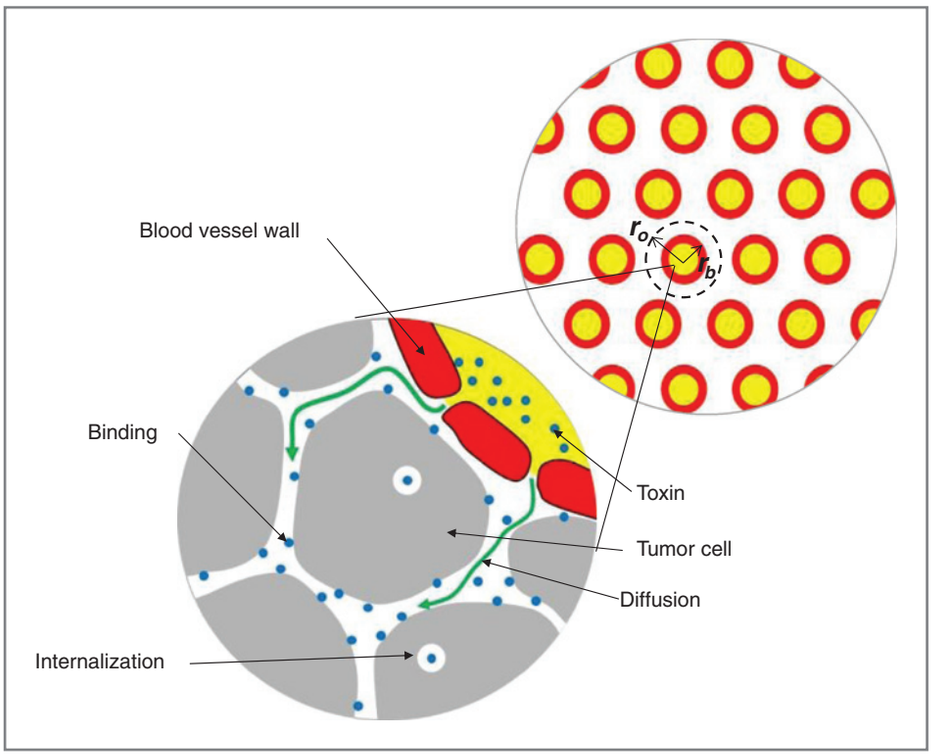

Figure 1. The tumor model. The tumor consists of a set of identical representative units (RU). Each RU is a sphere of radius of r_o. At the center of each RU is a blood vessel sphere of radius r_b. The toxin molecules (blue dots) in the plasma permeate through the blood vessel wall and diffuse into the ECS. The toxin molecules in the ECS bind the target antigens expressed on the cell surface and then are internalized by endocytosis.

average cell density and RIT concentrations of the material flowing in and out of the RUs are, in general, different from those within the RUs and makes appropriate corrections. These corrections are essential for precisely correct accounting of all RITs but were not made in the previous model.

The full details of the differential equations and their derivations are given in the Supplementary Materials and Methods.

Model parameters

The parameter values that were used for the model reported herein are given in the Supplementary Table S1. They are either taken from the earlier work (10) or obtained from, or by best fitting to, our published (20, 23–25) and unpublished experimental data.

Receptor shedding is a new feature of this model. The shedding rate constant k_s was estimated using the following unpublished *in vitro* experimental observation: When a cell culture containing 1.8×10^5 A431/H9 cells (19) in 150 μL of fresh medium was incubated for 5 hours, the mesothelin concentration in the medium was 8 nmol/L. Assuming that there are 1 million mesothelin molecules on the surface of each cell, this means that 80% of mesothelin is shed every hour. This *in vitro* rate was reduced by 50% ($k_s = 0.4$) for use in *in vivo* tumor in consideration of (i) the fact that the cells in tumor are packed more densely than in an *in vitro* culture system, which will reduce the access of sheddases to the substrate and (ii) a tumor tissue will contain a substantial amount of noncancer cells, which do not produce mesothelin. The model is not overly sensitive to this parameter; we could vary this parameter between 0.2 and 0.8 and refit other parameters to obtain similar quality fits to all the experimental data; none of the major conclusions of the model would change by this variation.

Results

The model gives a good fit with the experimental dose–response data

The model integrates the preclinical testing data of SS1P, most of which come from experiments in which SS1P was injected i.v. to treat mesothelin-expressing A431 tumors engrafted into nude mice. To be consistent with the clinical practice, SS1P was given every other day for a total of 3 doses. The change of tumor volume after treatment was tracked.

Figure 2A shows the tumor volume profiles calculated by the model to best fit the data from one such experiment (24). The fit is generally comparable with that of the original model (10) and good, given the simplicity of the tumor model used (see Materials and Methods) and the degree of reproducibility of the *in vivo* experimental tumor volume data. The same model also reproduces more recent data (refs. 20, 25; Fig. 2B and C) reasonably well, using the same set of parameter values except one, the Γ value (tumor growth rate constant in the absence of RIT), which was refit for each control data (without RIT administration). These results indicate that the current model, with its set of parameter values, has a predictive power on dose–response relationship in SS1P testing.

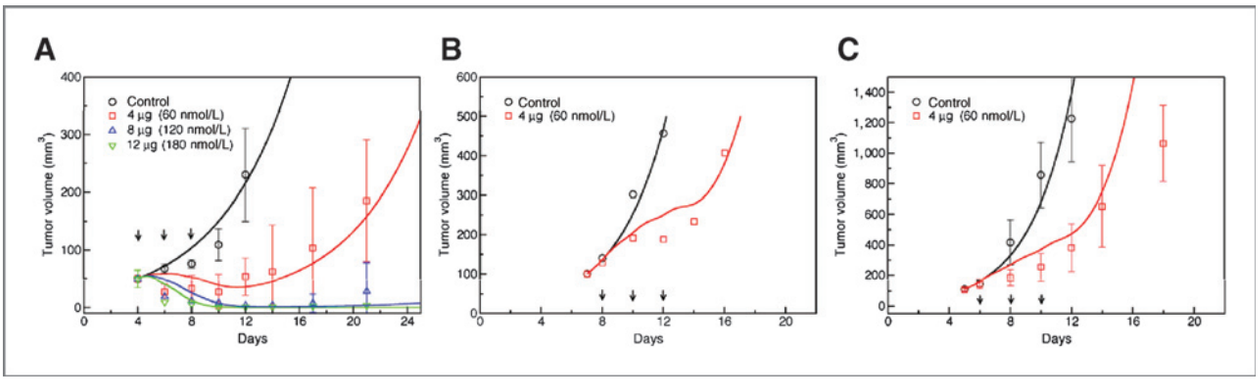

Figure 2. Calculated (lines) and experimental (symbols) tumor volume profiles. The black arrows indicate the times of RIT (SS1P) injection. A, experimental data of Onda and colleagues (24). The parameter values were chosen to give a best fit to this data set. B and C, experimental data of Zhang and colleagues (20, 25).

The model provides a full account of all RIT molecules in the tumor tissue at all times

Figure 3A shows time-dependent RIT quantities remaining or degraded in the EVS of the total tumor mass from the model of the experiment of Onda and colleagues (24) with 3 doses at 0.4 mg/kg. The amount of active RIT (red curve) quickly decreases after each injection as it is degraded (blue curve). The sum of the active and degraded RIT (purple curve) equals the total amount of RIT that crossed the blood vessel wall to enter the ECS of the tumor tissue up to each time point. Thus, the current model fully accounts for all the RIT that entered the EVS of the tumor tissue at all times. This precision is a significant improvement over the previous model (10).

The total amounts that crossed the blood vessel to enter the tumor EVS are 0.4% to 0.6% of the total injected dose (Table 1). These numbers are comparable with the 0.5% of the injected dose (4% per gram of tumor tissue of 120 mm^3 size) that Zhang and colleagues (25) found outside of the blood vessel in the A431/K5 tumor growing in nude mice 6 hours after a single injection. Obviously, larger tumors will take up more RIT.

Figure 3B shows the distribution of active and degraded RIT in different compartments of the tumor EVS at 6 different times for the same model of Fig. 3A. At 20 minutes after the first injection, 87% of the RIT that had entered the tumor EVS was bound to the surface antigen, 8.5% was bound to the shed antigen, and 3.6% had entered the type 1 (normal, as-yet

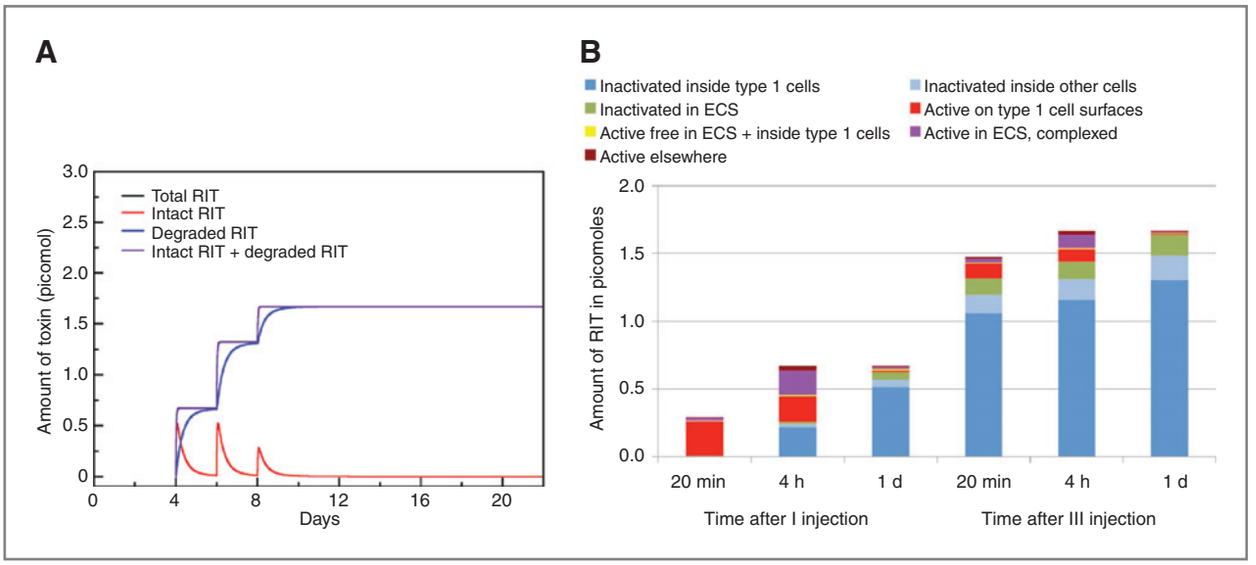

Figure 3. The total number of toxin molecules (in picomoles) in the tumor EVS for the model of the experiments of Onda and colleagues (24) at the 3 × 0.4 mg/kg dose, for a total of 375 picomoles for a 20-g mouse. A, currently active (intact RIT, red), inactivated (degraded RIT, blue), and the sum of the 2 (purple). The total number that exited from the blood vessel wall into the tumor EVS up to the indicated time (total RIT, black) is not visible because it precisely coincides with the purple curve. The 3 stepwise rises in the total amount of RIT correspond to 3 injections. The rises decrease in size for the second and third injections, even though the same amount was injected each time, because the tumor shrinks and fewer toxin molecules enter the tumor by the times of later injections. B, the amounts of active and degraded RIT in different compartments of the tumor EVS at 6 different times. Type 1 cells are the normal tumor cells that have not yet been intoxicated by RIT.

Table 1. Total amounts of RIT injected and calculated amounts that entered the tumor tissue by day 2

	Dosage[a]		
	4 μg	8 μg	12 μg
Total amount injected, nanomoles[b]	0.1875	0.375	0.5625
Total amount that entered tumor tissue, picomoles[c]	1.07 (0.57%)	1.67 (0.45%)	2.08 (0.37%)

[a]Calculated at day 2 after the last of the 3 RIT injections at 3 different indicated dose levels for the model of the experiments of Onda and colleagues (24).
[b]Assuming that a mouse weighs 20 g, the molecular weight of the RIT is 64 kDa, and the same dose was given 3 times.
[c]This is the cumulative amount that exited the blood vessel to enter the tumor ECS from the first injection to 2 days after the last injection. The number in parentheses is the percentage of the total injected dose. The fraction that enters the tumor tissue depends on the size of the tumor; it decreases at higher doses because tumor volume is smaller by the time of the second and third injections.

unintoxicated tumor) cells, approximately two thirds of which (2.3%) has been degraded. By 4 hours after the first injection, the total reached the final amount and no more RIT is entering the tumor EVS. Of the total amount that entered by this time, 38% has been degraded, most of which (32%) inside the type 1 cells. There is a large expansion of RIT bound to the shed antigen by this time (27%) at the expense of that bound to the surface antigen (28%). The amount active inside type 1 cells remains small (1.6%). One day after the first injection, 93% has been degraded, most (77%) inside the type 1 cells. But the amount active inside type 1 cells is maintained at 1.6%. The pattern after the third injection was similar, except that the total amount degraded was larger as the RIT from injections 2 and 4 days before had been degraded. By 1 day after the last injection, 98% of the RIT had been degraded, most of which (78%) was within type 1 cells. Thus, the tumor cells are the major sink of RIT.

Antigen shedding improves efficacy of RIT

Unless otherwise stated, our model assumes that antigen is shed. We obtain the nonshedding model by setting the shedding rate to zero and by correspondingly reducing the receptor synthesis and recycling rates so as to maintain the same number of antigen molecules on the cell surface as when the antigen is shed (see Supplementary Materials and Methods and Supplementary Fig. S2).

Figure 4 shows the calculated tumor volume profiles with time for 3 different models, each with an 8-μg (0.4 mg/kg for a 20-g mouse) dose given on days 4, 6, and 8. In the shedding model (solid blue curve), the tumor volume significantly shrinks after treatment, as we have seen in Fig. 2A. It is important to realize that the shed antigen in the ECS is not a sink for RIT in this model as the RIT is continually released from the antigen–RIT complexes with which free RIT is in a dynamic association–dissociation equilibrium.

When the shedding is maintained at the same rate, but the dissociation rate of the shed antigen–RIT complex is set to zero, the tumor keeps growing without shrinkage (red curve, "shedding without RIT release"). In this case, the shed antigen does act as a sink and efficiently reduces the amount of RIT available to bind the surface antigen, a necessary step before the RIT can kill the cell.

What is striking is the result for the nonshedding case in which there is no antigen in the ECS to serve as a sink. Quite unexpectedly, the RIT treatment in this case (broken blue curve) has a much more diminished antitumor effect than the shedding case (solid blue curve) and only slightly better than when the shed antigen acts as a sink (red curve). The number of cells killed in the nonshedding case is less than that in the shedding case at half the dose (data not shown). Thus, the model indicates unambiguously that antigen shedding makes the RIT substantially more effective. Preliminary calculations indicate that nearly identical results are obtained if the same amount of RIT is injected by continuous release over 6 days instead of 3 bolus injections every other day (data not shown).

Shed mesothelin helps overcome the binding site barrier by protecting RIT from degradation

One indication of the mechanism by which shed antigen enhances the effectiveness of RITs can be seen from Fig. 5A, which shows the fraction of unintoxicated type 1 cells as a function of the distance from the blood vessel center at

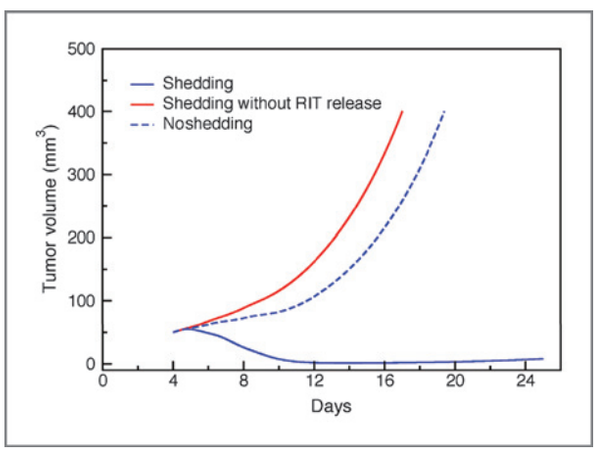

Figure 4. The tumor volume profiles for 3 different models. The cases of surface antigen shedding and not shedding are denoted as "shedding" (blue solid line) and "no shedding" (blue broken line), respectively. The shedding case in which the complexed RIT molecules in the ECS do not dissociate is denoted as "shedding without RIT release" (red line). The calculations are for the model of the experiment of Onda and colleagues (24) at the 0.4-mg/kg dose.

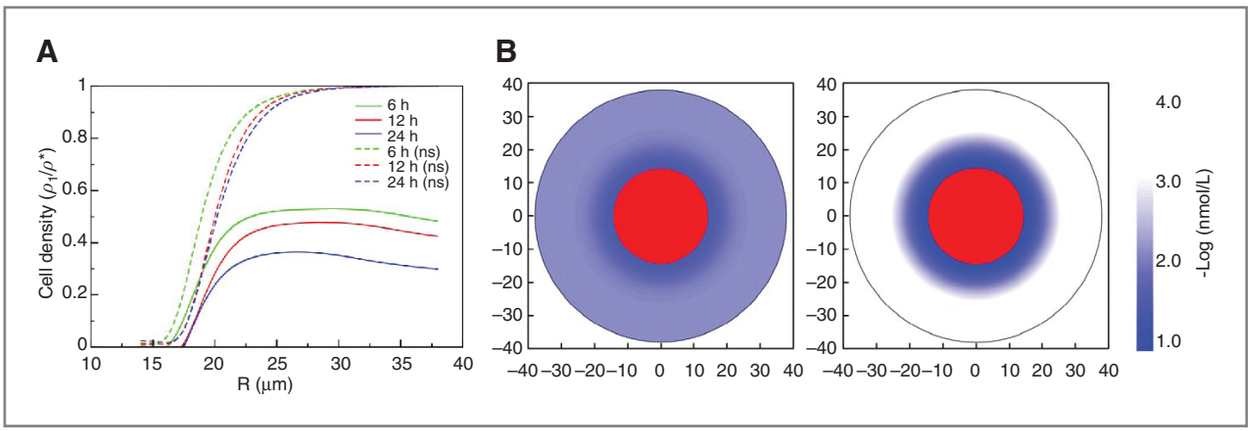

Figure 5. A, the normalized density of unintoxicated (type 1) cells versus radial distance from the center of the RU at indicated times after the last (third) injection for shedding (solid lines) and nonshedding (ns; broken lines) cases. When the normalized density is less than 1, it means that there are intoxicated (type 2) and dead (type 3) cells. The calculations are for the model of the experiment of Onda and colleagues (24) at 0.4 mg/kg dose. B, free RIT concentration in ECS at 6 hours after the last injection for shedding (left) and nonshedding (right) cases for the same model as in (A). The black outer circle indicates the boundary of the RU. The red filled circle at the center represents the blood vessel. Its size is chosen such that its volume constitutes 5% of the RU. The numbers at the bottom and left margins indicate the radial distance from the center of the RU in μm units. The RIT concentration is indicated by the intensity of the blue color. The color index at right gives the correspondence between the color intensity and the concentration, which is given in units of −log_base_10 (nmo/L).

different times. When the shedding is not allowed (broken lines), cell intoxication and killing, as indicated by the deviation of the plotted values from 1, are limited to the immediate vicinity of the blood vessel. This is consistent with what is expected from the "binding site barrier" model (13, 14), according to which RIT binding to the target antigen near the blood vessel hinders the penetration of RIT into tumor tissue. This strongly contrasts with the shedding case (solid lines) wherein the intoxication and killing are widespread throughout the tumor volume. These data suggest that shed antigen helps carry the RIT away from the blood vessel and circumvent the binding site barrier.

The radial distribution of the concentration of free RIT in ECS directly shows this to be the case. Indeed, Fig. 5B shows that the free RIT concentration decreases sharply beyond about 20 μm in the nonshedding case (right) but is maintained, albeit at a low level, in the shedding case (left).

In contrast, the concentration of the shed antigen–RIT complexes in ECS displays virtually no radial distance dependence after initial first hour of the last (third) injection (Supplementary Fig. S3). This is because the complexed RIT does not bind the surface antigen and because the diffusion of these molecules, although slower than the smaller RIT molecules, is still fast enough for them to permeate the entire volume of the tumor tissue in a few hours. In effect, the shed antigen serves as a carrier of RIT, protecting it from excessively binding to the surface antigen during its transport to the distant parts of the tumor tissue. Wherever they are transported, these RIT–antigen complexes release RIT continually at a low level, in a dynamic association–dissociation equilibrium process, making them available to bind the surface antigen.

Antigen shedding causes favorable RIT distribution among tumor cells

There is another mechanism by which the antigen shedding enhances RIT efficacy. Figure 6A shows the number of internalized active RIT molecules in each cell type for both shedding (solid lines) and nonshedding (broken line) cases. Antigen shedding increases the number of RIT molecules in type 1 cells (solid red line is above the broken red line), but decreases the number in type 2 or 3 cells (solid green and blue lines are below their respective broken lines). This RIT distribution pattern favors the antitumor effect because more RIT molecules are directed to unintoxicated (type 1) tumor cells instead of being wasted in intoxicated (type 2) or dead (type 3) cells.

How does shedding bring about these desirable features? Figure 6B shows the total number of surface antigen molecules per cell for each cell type. For both the shedding and nonshedding cases, the total number of antigen molecules on the surface of an unintoxicated tumor cell is constant and the same (red line—solid and broken lines overlap). The number decreases in an intoxicated cell (broken green line) because the surface antigen molecules are continually endocytosed and degraded, but are not replenished because of the arrest of new protein synthesis. When the antigen is shed, the number decreases even more (solid green line). The dead cells show the accumulated effect (blue curves). Obviously, less surface receptor molecules translate into less RIT molecules inside the cell.

Discussion

The model presented here is based on the model we described earlier (10), but we improved it by rewriting the entire set of differential equations to make the model quantitatively more precise, to recognize 3 rather than 2 cell types, and most importantly by including the effect of antigen shedding, which was not included in the original model.

An important advantage of this model is that it can handle tumors of any size and yields total tumor volume information dynamically while considering only one representative unit of a

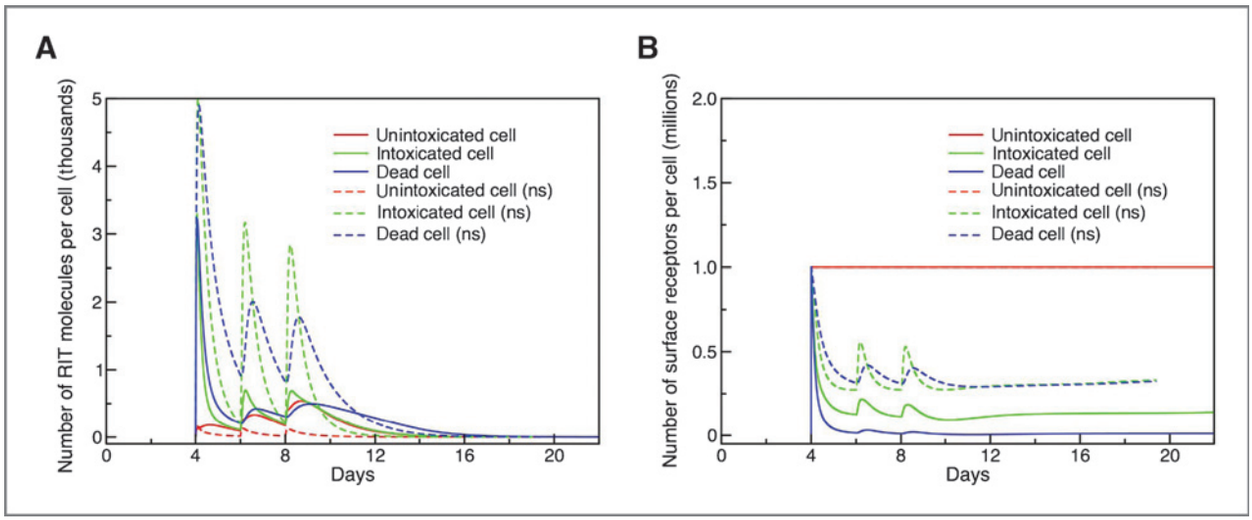

Figure 6. Time profiles of the number of internalized RIT (A) and surface antigen (B) molecules per cell for each cell type in the shedding (solid lines) and the nonshedding (ns; broken lines) cases. The 3 cell types are unintoxicated (cell 1), intoxicated (cell 2), and dead (cell 3) cells. The calculations are for the model of the experiment of Onda and colleagues (24) at the 0.4-mg/kg dose.

modest and constant size. Because the model assumes that the total cell density is uniform and unchanged, this is not a good model for poorly vascularized, necrotic regions of the tumor. However, the efficacy of RIT is an issue for well vascularized, rapidly growing tumor; it may be less important for slowly growing, necrotic regions of a tumor. Also, although the cell density is assumed constant for any one tumor model, one can study the effect of density changes by doing the calculations on many tumor models with varying cell densities. The density variation can be caused, for example, by killing cells with other agents such as paclitaxel or saponin (see later).

This model, like the earlier model, reproduces the experimental tumor volume changes upon administration of different amounts of RIT (Fig. 2). In addition, it gives a full accounting of all RIT administered at all times (Fig. 3). We note, for example, that more than 70% of the RIT that entered the tumor EVS was degraded (or made inactive in some fashion) in the endosomal compartment within the normal, yet-to-be intoxicated tumor cells. That the passage through the endosomal compartments within the tumor cells presents a major hurdle in the delivery of macromolecular therapeutic agents has been well recognized (see for example, Ogata and colleagues; ref. 26 and Belting and Wittrup; ref. 27) The total number of RIT molecules in a yet-to-be-intoxicated tumor cell is less than 1,000 molecules (Fig. 6A), which is consistent with the experimental finding of Kreitman and Pastan (23).

The main finding of this study is that antigen shedding enhances the efficacy of RIT, contrary to the suggestion some of us made earlier (see later). Shedding improves the RIT efficacy in 2 ways. One mechanism is through circumventing the binding site barrier (13, 28), which is recognized as one of the main reasons for the nonhomogeneous distribution of therapeutic agents in the tumor tissue (14). Graff and Wittrup (3) concluded from theoretical considerations that the presence of reversible binders (such as the shed mesothelin) will retard the penetration of RIT by hours, not by days. However, tumor cells are the main sinks of RIT, as most of the RIT is lost by being captured by the cells (target-mediated drug disposition; ref. 29). When sinks are present, the penetration can be delayed by days or, in principle, forever. Here, we found that antigen shedding is an effective, natural way of circumventing this barrier. The shed antigen acts as a protective reservoir, which carries RIT into spaces far removed from the blood vessel without excessive binding to the surface antigens in transit and which preserves it for a long time after the last injection. This is consistent with the expectation that a nonbinder, as the shed antigen–RIT complex is, will spread throughout the tumor tissue in hours (4) or less (14). Second, shedding reduces wasteful binding of RIT to the already intoxicated cells by reducing the surface antigen concentration on these cells. Indeed, we have observed experimentally that incubation of cells with RIT can reduce cell surface mesothelin by 90% within 3 hours (unpublished data). This reduction must be due to the fact that RIT induces protein synthesis inhibition and the surface mesothelin is no longer replenished while it is being lost by shedding as well as by endocytosis.

There is strong experimental evidence that indicates that a RIT reservoir exists in the tumor tissue. Previously, we intravenously injected dye-labeled mutant SS1P into mice bearing mesothelin-expressing tumors (20). The mutation (E553D) inactivates the toxin part of the molecule so that it does not kill cells. We found that the peak of intracellular staining appeared 6 hours after SS1P was cleared from the blood (Fig. 3A in Zhang and colleagues; ref. 20). This delay suggests that a reservoir in the tumor supplies SS1P long after the blood supply has been depleted. The model presented here is consistent with this data and indicates that the RIT–mesothelin complex in tumor ECS is this reservoir. The model is also consistent with the report of Junghans and colleagues (9) that the shed antigen–antibody complex can supply the antibody to bind leukemic cells and solid tumors when free antibody is depleted.

Some of us observed that mesothelin was shed in the human tumor growing in mice and that administration of paclitaxel, which exerts synergistic effect with SS1P, reduced the concentration of shed mesothelin. From this observation, we surmised that the synergy was due to the reduction of shed antigen concentration and that shed antigen must hinder the action of SS1P (20, 21, 30). However, the synergistic effect of paclitaxel can arise from a different mechanism (see later), independent of the reduction in the shed antigen concentration. More recently, some of us showed that reducing shedding significantly improved the cytotoxicity of immunotoxin SS1P (19). However, this is an observation made on an *in vitro* cell culture system, in which the beneficial effect of shed antigen acting as a protective carrier and reservoir of RIT is not expected to exist as it does in a solid tumor.

Some suggestions on improving the potency of RITs as anticancer agent can be made based on the results that this model produced. For example, the benefit of antigen shedding should be considered in selecting potential targets. One could also consider using the antigen or antigen analogues in combination to serve as the carrier and protective reservoir of the RIT. Adding competing (nontoxic) antibody in judicious amounts can also help as it would increase the concentration of RIT in the reservoir.

The model suggests other possible combination therapy strategies. For example, RIT that enters the tumor tissue is lost most during the passage through the endosome. Any method that will reduce the degradation in this step can be expected to improve the efficacy of RITs. One possibility is to introduce a disulfide bond into the RIT to improve its stability, as was done recently by Liu and colleagues (31). Another possibility is to use agents in combination with RIT that will increase translocation efficiency. Li and colleagues (6) suggest a number of methods to promote escape from endosome. The photochemical internalization (PCI) technique has also been shown to enhance the cytotoxicity of immunotoxins by facilitating the release of the toxin from endolysosomal compartments to the cell cytosol (32). Another possible agent is ABT-737, which has recently been shown to enhance the cytotoxicity of immunotoxins, probably also by increasing the amount of translocation from endoplasmic reticulum to the cytosol (33). In addition, the model should be a useful tool for discovering possible mechanism(s) by which agents such as paclitaxel (ref. 25; see earlier) and saponin (34) exert their synergistic effect when used in combination with immunotoxins. For example, it is possible that these agents kill cells and reduce the cell density of the tumor tissue. Lower density can help RIT to penetrate deeper into the tumor tissue and increase its efficacy. Such a conjecture can be tested by calculation before an experimental proof.

Our model should be useful in studying the delivery efficacy of antibody–drug conjugates (ADC), many of which are in the advanced stages of clinical trials (35). ADCs share the same targeting mechanism with RITs. Also, this model and the conclusions derived from it can be applied to other cancer targets, such as Her-2/neu, CEA, PSA. They all experience active shedding, and many agents against them are under development (8).

The finding that antigen shedding improves the delivery of RITs may have a broader biologic implication. The binding site barrier will exist even for natural signaling molecules if they get destroyed upon binding to their receptors. It seems possible that some such receptors are shed to improve the range and duration of the signaling molecules. Obviously, this expectation, like all other predictions from a mathematical model, needs to be proved by actual experiments.

Disclosure of Potential Conflicts of Interest

No potential conflicts of interest were disclosed.

Authors' Contributions

Conception and design: Y. Pak, B. Lee
Development of methodology: Y. Pak, Y. Zhang, B. Lee
Acquisition of data (provided animals, acquired and managed patients, provided facilities, etc.): Y. Pak, Y. Zhang, I. Pastan, B. Lee
Analysis and interpretation of data (e.g., statistical analysis, biostatistics, computational analysis): Y. Pak, I. Pastan, B. Lee
Writing, review, and/or revision of the manuscript: Y. Pak, Y. Zhang, I. Pastan, B. Lee
Administrative, technical, or material support (i.e., reporting or organizing data, constructing databases): Y. Pak, B. Lee
Study supervision: B. Lee

Acknowledgments

The authors thank Richard Beers for providing unpublished data on the SS1P association and dissociation rates with mesothelin.

Grant Support

Y. Pak thanks Pusan National University Research Fund for the financial support. This research was supported in part by the Intramural Research Program of the NIH, National Cancer Institute, Center for Cancer Research for Y. Zhang, I. Pastan, and B. Lee.

The costs of publication of this article were defrayed in part by the payment of page charges. This article must therefore be hereby marked *advertisement* in accordance with 18 U.S.C. Section 1734 solely to indicate this fact.

Received December 1, 2011; revised March 20, 2012; accepted April 13, 2012; published OnlineFirst May 4, 2012.

References

1. Adams GP, Weiner LM. Monoclonal antibody therapy of cancer. Nat Biotechnol 2005;23:1147–57.
2. Oldham RK, Dillman RO. Monoclonal antibodies in cancer therapy: 25 years of progress. J Clin Oncol 2008;26:1774–7.
3. Graff CP, Wittrup KD. Theoretical analysis of antibody targeting of tumor spheroids: importance of dosage for penetration, and affinity for retention. Cancer Res 2003;63:1288–96.
4. Jain RK. Delivery of molecular and cellular medicine to solid tumors. Adv Drug Deliv Rev 2001;46:149–68.
5. Jang SH, Wientjes MG, Lu D, Au JL. Drug delivery and transport to solid tumors. Pharm Res 2003;20:1337–50.
6. Li Y, Wang J, Wientjes MG, Au JL. Delivery of nanomedicines to extracellular and intracellular compartments of a solid tumor. Adv Drug Deliv Rev 2011;64:29–39.
7. Thurber GM, Schmidt MM, Wittrup KD. Factors determining antibody distribution in tumors. Trends Pharmacol Sci 2008;29:57–61.
8. Kulasingam V, Diamandis EP. Strategies for discovering novel cancer biomarkers through utilization of emerging technologies. Nat Clin Pract Oncol 2008;5:588–99.
9. Junghans RP, Carrasquillo JA, Waldmann TA. Impact of antigenemia on the bioactivity of infused anti-Tac antibody: implications for dose

selection in antibody immunotherapies. Proc Natl Acad Sci U S A 1998;95:1752–7.
10. Chen KC, Kim J, Li X, Lee B. Modeling recombinant immunotoxin efficacies in solid tumors. Ann Biomed Eng 2008;36:486–512.
11. Jackson TL. Vascular tumor growth and treatment: consequences of polyclonality, competition and dynamic vascular support. J Math Biol 2002;44:201–26.
12. Jackson TL, Byrne HM. A mathematical model to study the effects of drug resistance and vasculature on the response of solid tumors to chemotherapy. Math Biosci 2000;164:17–38.
13. Fujimori K, Covell DG, Fletcher JE, Weinstein JN. A modeling analysis of monoclonal antibody percolation through tumors: a binding-site barrier. J Nucl Med 1990;31:1191–8.
14. Thurber GM, Schmidt MM, Wittrup KD. Antibody tumor penetration: transport opposed by systemic and antigen-mediated clearance. Adv Drug Deliv Rev 2008;60:1421–34.
15. Hassan R, Ho M. Mesothelin targeted cancer immunotherapy. Eur J Cancer 2008;44:46–53.
16. Hassan R, Bullock S, Premkumar A, Kreitman RJ, Kindler H, Willingham MC, et al. Phase I study of SS1P, a recombinant anti-mesothelin immunotoxin given as a bolus I.V. infusion to patients with mesothelin-expressing mesothelioma, ovarian, and pancreatic cancers. Clin Cancer Res 2007;13:5144–9.
17. Kreitman RJ, Hassan R, Fitzgerald DJ, Pastan I. Phase I trial of continuous infusion anti-mesothelin recombinant immunotoxin SS1P. Clin Cancer Res 2009;15:5274–9.
18. Trial NC. SS1P and pentostatin plus cyclophosphamide for mesothelioma. Bethesda, MD: National Institutes of Health Clinical Center; 2012. Available from: http://www.cancer.gov/clinicaltrials.
19. Zhang Y, Chertov O, Zhang J, Hassan R, Pastan I. Cytotoxic activity of immunotoxin SS1P is modulated by TACE-dependent mesothelin shedding. Cancer Res 2011;71:5915–22.
20. Zhang Y, Hansen JK, Xiang L, Kawa S, Onda M, Ho M, et al. A flow cytometry method to quantitate internalized immunotoxins shows that taxol synergistically increases cellular immunotoxins uptake. Cancer Res 2010;70:1082–9.
21. Zhang Y, Pastan I. High shed antigen levels within tumors: an additional barrier to immunoconjugate therapy. Clin Cancer Res 2008;14:7981–6.
22. Juweid M, Neumann R, Paik C, Perez-Bacete MJ, Sato J, van Osdol W, et al. Micropharmacology of monoclonal antibodies in solid tumors: direct experimental evidence for a binding site barrier. Cancer Res 1992;52:5144–53.
23. Kreitman RJ, Pastan I. Accumulation of a recombinant immunotoxin in a tumor *in vivo*: fewer than 1000 molecules per cell are sufficient for complete responses. Cancer Res 1998;58:968–75.
24. Onda M, Nagata S, Tsutsumi Y, Vincent JJ, Wang Q, Kreitman RJ, et al. Lowering the isoelectric point of the Fv portion of recombinant immunotoxins leads to decreased nonspecific animal toxicity without affecting antitumor activity. Cancer Res 2001;61:5070–7.
25. Zhang Y, Xiang L, Hassan R, Paik CH, Carrasquillo JA, Jang BS, et al. Synergistic antitumor activity of taxol and immunotoxin SS1P in tumor-bearing mice. Clin Cancer Res 2006;12:4695–701.
26. Ogata M, Chaudhary VK, Pastan I, FitzGerald DJ. Processing of Pseudomonas exotoxin by a cellular protease results in the generation of a 37,000-Da toxin fragment that is translocated to the cytosol. J Biol Chem 1990;265:20678–85.
27. Belting M, Wittrup A. Developments in macromolecular drug delivery. Methods Mol Biol 2009;480:1–10.
28. Weinstein JN, Eger RR, Covell DG, Black CD, Mulshine J, Carrasquillo JA, et al. The pharmacology of monoclonal antibodies. Ann N Y Acad Sci 1987;507:199–210.
29. Mager DE. Target-mediated drug disposition and dynamics. Biochem Pharmacol 2006;72:1–10.
30. Zhang Y, Xiang L, Hassan R, Pastan I. Immunotoxin and Taxol synergy results from a decrease in shed mesothelin levels in the extracellular space of tumors. Proc Natl Acad Sci U S A 2007;104:17099–104.
31. Liu W, Onda M, Kim C, Xiang L, Weldon JE, Lee B, et al. A recombinant immunotoxin engineered for increased stability by adding a disulfide bond has decreased immunogenicity. Protein Eng Des Sel 2012;25:1–6.
32. Yip WL, Weyergang A, Berg K, Tonnesen HH, Selbo PK. Targeted delivery and enhanced cytotoxicity of cetuximab-saporin by photochemical internalization in EGFR-positive cancer cells. Mol Pharm 2007;4:241–51.
33. Traini R, Ben-Josef G, Pastrana DV, Moskatel E, Sharma AK, Antignani A, et al. ABT-737 overcomes resistance to immunotoxin-mediated apoptosis and enhances the delivery of pseudomonas exotoxin-based proteins to the cell cytosol. Mol Cancer Ther 2010;9:2007–15.
34. Bachran C, Durkop H, Sutherland M, Bachran D, Muller C, Weng A, et al. Inhibition of tumor growth by targeted toxins in mice is dramatically improved by saponinum album in a synergistic way. J Immunother 2009;32:713–25.
35. Sapra P, Hooper AT, O'Donnell CJ, Gerber HP. Investigational antibody drug conjugates for solid tumors. Expert Opin Investig Drugs 2011;20:1131–49.